

Shape Control of CdS Nanocrystals in One-Pot Synthesis

Ken-Tye Yong,^{†,‡} Yudhisthira Sahoo,^{†,§} Mark T. Swihart,^{*,†,‡} and Paras N. Prasad^{†,§}

Institute for Lasers, Photonics, and Biophotonics, Department of Chemical and Biological Engineering, and Department of Chemistry, University at Buffalo, The State University of New York, Buffalo, New York 14260-4200

Received: September 28, 2006; In Final Form: November 21, 2006

We report here straightforward solution-phase methods of preparing CdS NCs with a wide variety of morphologies, starting with oleylamine as the surfactant or capping agent, and varying the reaction conditions. We have systematically investigated the effects of temperature, precursor concentration, growth time, addition of metal nanoparticles, addition of cosurfactants, and acidification of the reaction medium on the growth of CdS NCs. These parameters have a tremendous impact on the morphology of the nanocrystals, allowing the controlled synthesis of a series of shapes including nanorods, bipods, tripods, tetrapods, nanocubes, nanowires, chain-like nanostructures, and nanoplatelets. At 100 °C, in the absence of secondary additives, we observed the nucleation of zinc blend CdS cores, followed by the growth of wurtzite arms to produce rods, bipods, and tripods. The addition of tetradecylphosphonic acid suppressed the growth of the wurtzite arms, resulting in zinc blend cubic nanocrystals. The addition of gold nanoparticles or acidification of the reaction medium led to nucleation and anisotropic growth of the wurtzite polymorph.

Introduction

Many physical properties of nanostructured semiconductors depend strongly on their size, shape, and crystal structure.¹ Thus, the development of well-controlled synthetic methods for tailoring nanocrystal shape and elucidation of the mechanisms by which the size and shape of the nanocrystals can be controlled are important issues in nanomaterials chemistry. CdS has a Bohr radius of 2.4 nm² and direct band gap of 2.4 eV³ and is used in photovoltaics, in light-emitting diodes for flat-panel displays, and in other optical devices based on its nonlinear properties.^{4,5} CdS has been extensively studied during the past few decades.^{6–12}

Various methods of manipulating the shape and size of CdS nanocrystals have been reported. For example, CdS nanowires have been fabricated by laser ablation with a metal catalyst as seeds,¹³ by a solution process,¹⁴ by a thermal evaporation process,^{15–18} and by a templating technique.^{19,20} CdS nanorods were prepared by solution techniques using structure-directing agents, microemulsion techniques, microwave techniques, and arrested precipitation.^{21–25} Star-like CdS NCs were prepared from a lyotropic triblock copolymer solution system.²⁶ CdS nanotetrahedrons, pencil-shaped nanorods, tetrapods, prickly spheres, and hexagonal nanoprisms have been prepared using mixed solvents of ethylenediamine and ethylene glycol under solvothermal conditions.²⁷ CdS nanobelts have been grown by vapor-phase transport.²⁸

The controlled synthesis of NCs of various shapes is an important step in the development of new nanoscale electronic and photonic devices. Although CdS nanocrystals with a wide variety of shapes have been achieved by individually tailored routes, there has not been a general colloidal route for producing CdS NCs of many different shapes using the same basic

technique and the same set of starting reagents. In view of this, we report here a general synthetic method that can be modified to yield a variety of shapes of CdS NCs. These NCs are potentially useful in the study of optical interference and coupling, and many other collective nonlinear effects, as well as for components of new electronic or photonic devices.

In this work, we have attempted to develop a broad experimental protocol to obtain anisotropic CdS nanostructures of different shapes, using a hot colloidal method, starting from a single surfactant. Following this, variations of the reaction conditions, including the independent addition of small amounts of additives such as tetradecylphosphonic acid (TDPA), cetyltrimethylammonium bromide (CTAB), trioctylphosphine oxide (TOPO), gold (Au) nanoparticles, and hydrochloric acid have been carried out to examine their effects. These parameters have tremendous impact on the morphology of the nanocrystals, yielding a library of shapes including nanorods, bipods, tripods, tetrapods, nanocubes, nanowires, and nanoplatelets.

Materials and Methods

Materials. Cadmium chloride (CdCl₂), oleylamine, sulfur, tetraoctylammonium bromide (98%) (TOAB), hydrogen tetrachloroaurate(III) trihydrate (HAuCl₄·3H₂O), sodium borohydride, cetyltrimethylammonium bromide (CTAB), and dodecylamine were purchased from Aldrich; hydrochloric acid (HCl) was from Baker; and tetradecylphosphonic acid (TDPA) was from Alfa Aesar. All chemicals were used as received. All solvents (hexane, toluene, and ethanol) were of reagent grade and were used without further purification.

Typical Synthesis Procedures. (a) Synthesis of Au Nanoparticles. Au nanoparticles dispersible in organic solutions were prepared by the well-known two-phase reduction method.^{29,30} A total of 20 mL of a bright yellow 5 mM HAuCl₄ solution was mixed with 10 mL of a 25 mM TOAB toluene solution. The mixture was vigorously stirred for 15 min. Two immiscible layers immediately formed, with an orange/red organic phase

* Corresponding author. Tel.: (716) 645-2911 ext. 2205. Fax: (716) 645-3822. E-mail: swihart@eng.buffalo.edu.

[†] Institute for Lasers, Photonics, and Biophotonics.

[‡] Department of Chemical and Biological Engineering.

[§] Department of Chemistry.

on the top and a clear/slightly orange tinted aqueous phase at the bottom. The organic phase was separated into a glass vial, and a solution of 0.12 g of dodecylamine in 5 mL of toluene was added to it, followed by dropwise addition of 5 mL of a 0.1 M sodium borohydride aqueous solution to the stirring reaction mixture. An instantaneous color change of the organic phase was observed from an orange/red to a deep-red color. The stirring was continued for 30 min. Following this, the organic phase containing gold nanoparticles was separated from the aqueous phase and adjusted to 20 mL by the addition of toluene.

(b) Synthesis of Spherical CdS Nanocrystals. The synthesis method was adapted from that presented by Joo et al.³¹ An oleylamine–sulfur solution was prepared by dissolving 0.1926 g of sulfur (6 mmol) in 5 mL of oleylamine. Separately, 1 mmol of cadmium chloride was dissolved in 10 mL of oleylamine. The CdCl₂ solution was heated at 175 °C for 20–35 min under argon flow, and then the oleylamine–sulfur solution was injected under gentle stirring into the hot reaction mixture. The reaction mixture was held at 175 °C and stirred for ~3 h, and then an aliquot was removed by a syringe and injected into a large volume of toluene at room temperature to quench the reaction. The NCs were separated from the toluene solution by the addition of ethanol and centrifugation. The yellow NC precipitate could be redispersed in various organic solvents including hexane, toluene, and chloroform.

(c) Synthesis of CdS Nanorods, Bipods, and Tripods. An oleylamine–sulfur solution was prepared by dissolving 0.1926 g of sulfur (6 mmol) in 5 mL of oleylamine. Separately, 1 mmol of cadmium chloride was dissolved in 10 mL of oleylamine. The CdCl₂ solution was heated at 100 °C for 20–35 min under an argon flow, and then the oleylamine–sulfur solution was injected under gentle stirring into the hot reaction mixture. The reaction mixture was held at 100 °C and stirred for ~19 h.

(d) High-Yield Synthesis of CdS Tetrapods and Tripods. An oleylamine–sulfur solution was prepared by dissolving 0.926 g of sulfur (30 mmol) in 20 mL of oleylamine. Separately, 5 mmol of cadmium chloride was dissolved in 10 mL of oleylamine. The CdCl₂ solution was heated at 100 °C for 20–35 min under an argon flow, and then the oleylamine–sulfur solution was injected under stirring into the hot reaction mixture. The reaction mixture was held at 100 °C and stirred for ~19 h.

(e) Synthesis of CdS “Candy Corn” Nanocrystals. A total of 30 mmol of sulfur was added to 10 mL of oleylamine and heated to 70 °C for 20–35 min under argon flow to fully dissolve the sulfur. Separately, 10 mmol of cadmium chloride in 15 mL of oleylamine was heated to 100 °C, forming a homogeneous and clear solution. The Cd–oleylamine solution was then injected into the hot sulfur–oleylamine solution. The reaction mixture was held at 100 °C and stirred for ~19 h.

(f) Synthesis of CdS Tetrapods with Wire-Like Arms. An oleylamine–sulfur solution was prepared by dissolving 0.1926 g of sulfur (6 mmol) in 5 mL of oleylamine. Separately, 2 mmol of cadmium chloride and 0.1 g of tetradecylphosphonic acid (TDPA) were dissolved in 10 mL of oleylamine. The CdCl₂/TDPA solution was heated at 100 °C for 20–35 min under an argon flow, and then the oleylamine–sulfur solution was injected under stirring into the hot reaction mixture. The reaction mixture was held at 100 °C and stirred for ~19 h.

(g) Synthesis of CdS Nanocubes. Cubic CdS NCs were prepared following the same procedure described previously in section f, except that 1 mmol of CdCl₂ and 0.25 g of TDPA were used.

(h) Synthesis of CdS Chain-Like Nanostructures. An oleylamine–sulfur solution was prepared by dissolving 0.1926 g of sulfur (6 mmol) in 5 mL of oleylamine. Separately, 1 mmol of cadmium chloride and 5 g of CTAB were dissolved in 10 mL of oleylamine. The CdCl₂/CTAB solution was heated to 140 °C for 20–35 min under an argon flow, and then the oleylamine–sulfur solution was injected under stirring into the hot reaction mixture. The reaction mixture was held at 140 °C and stirred for ~19 h.

(i) High-Yield Synthesis of CdS Nanorods with Aspect Ratio of ~6.2. An oleylamine–sulfur solution was prepared by dissolving 0.1926 g of sulfur (6 mmol) in 5 mL of oleylamine. Separately, 1 mmol of cadmium chloride and 1 g of TOPO were dissolved in 10 mL of oleylamine. The CdCl₂/TOPO solution was heated to 100 °C for 20–35 min under an argon flow, and then the oleylamine–sulfur solution was injected under stirring into the hot reaction mixture. The reaction mixture was held at 100 °C and stirred for ~19 h.

(j) Synthesis of CdS Nanoplatelets. An oleylamine–sulfur solution was prepared by dissolving 0.1926 g of sulfur (6 mmol) in 5 mL of oleylamine. Separately, 1 mmol of cadmium chloride and Au nanoparticles (~4 nm diameter, corresponding to ~0.025 mmol of metal atoms) in 10 mL of oleylamine were heated to 175 °C for ~20 min under an argon flow. Then, the oleylamine–sulfur solution was injected into the hot reaction mixture. The reaction mixture was held at 175 °C and stirred for ~19 h.

(k) Au-Seeded Synthesis of CdS Nanorods, Bipods, Tripods, Tetrapods, and Quasi-Spherical NCs. CdS NCs were prepared following the same procedure described previously in section j, except that the growth temperature was 100 °C rather than 175 °C.

(l) High-Yield Synthesis of Highly Uniform CdS Nanorods with an Aspect Ratio of 5. CdS NCs were prepared following the procedure described previously in panel c, except that ~5.5 mmol of HCl was added to the reaction mixture before heating.

A summary of reaction conditions used for different shapes and sizes of CdS NCs is presented in Table 1.

Characterization Methods. (a) UV–Vis Absorbance. The absorption spectra were collected using a Shimadzu model 3101PC UV–vis NIR scanning spectrophotometer over a wavelength range from 300 to 800 nm. The samples were measured against hexane as a reference. All samples were dispersed in hexane and loaded into a quartz cell for measurement.

(b) Transmission Electron Microscopy (TEM). Transmission electron microscopy (TEM) images were obtained using a JEOL model JEM-100CX microscope at an acceleration voltage of 80 kV. The specimens were prepared by drop-coating the sample dispersion onto an amorphous carbon-coated 300 mesh copper grid, which was placed on filter paper to absorb excess solvent.

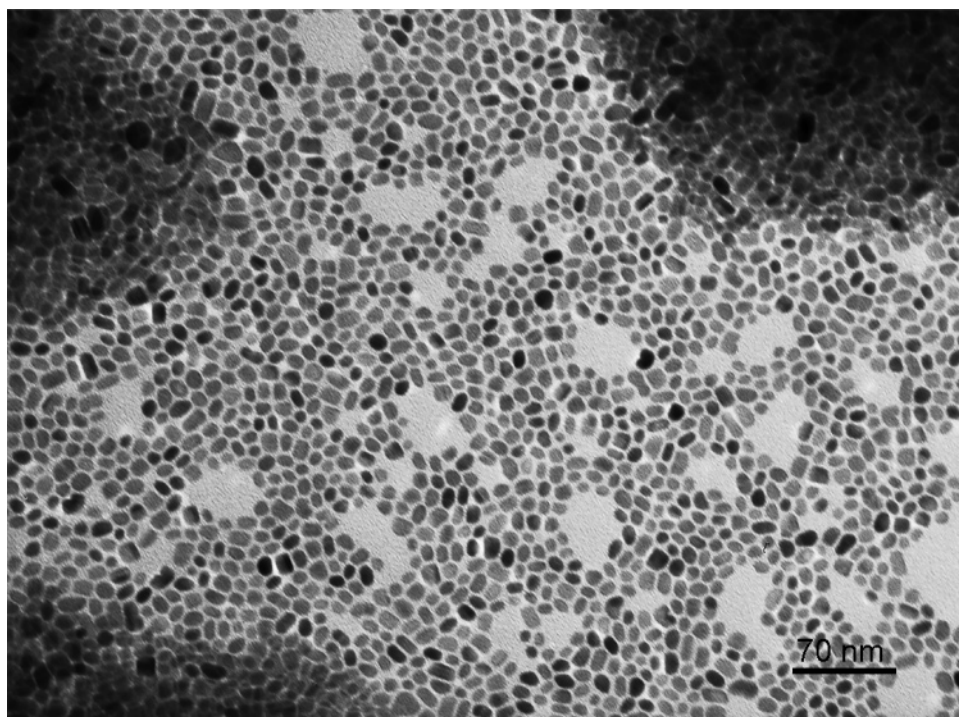
(iii) High-Resolution Transmission Electron Microscopy (HRTEM). Transmission electron microscopy (TEM) images were obtained using a JEOL model JEM 2010 microscope at an acceleration voltage of 200 kV or by using the Philips CM300 microscope at the National Center for Electron Microscopy. The specimens were prepared by drop-coating the sample dispersion onto an amorphous carbon-coated 300 mesh copper grid, which was placed on filter paper to absorb excess solvent.

(c) X-ray Diffraction (XRD). X-ray powder diffraction patterns were recorded using a Siemens D500 diffractometer, with Cu K α radiation. A concentrated nanocrystal dispersion was drop-cast onto a quartz plate for measurement.

TABLE 1: Summary of Synthesis Conditions and Resulting Morphologies

CdCl ₂ (mmol)	S (mmol)	solvent volume (mL)	temp (°C)	reaction time (h)	additives	shape	dimensions (nm) and predominant phase	yield (%)
1	6	15	175	~3		spherical	12; mixed	~100 ^e
1	6	15	175	~19		irregular shapes	mixed	
1	6	15	100	~19		nanorods, bipods, and tripods	16.7; ^a 5.5; ^b mixed	~70 ^e
5	30	30	100	~19		tetrapods and tripods	mixed	~65 ^e
10	30	25	100	~19		nano-“candy corns”	mixed	~80 ^e
2	6	15	100	~19	0.1 g of TDPA	tetrapods with wire-like arms		<10 ^e
1	6	15	100	~19	0.25 g of TDPA	nanocubes	12; ^d zinc blend	~85 ^e
1	6	15	140	~19	5.0 g of CTAB	chain-like nanostructure		~90 ^e
1	6	15	100	~19	1.0 g of TOPO	nanorods	23.4; ^a 3.8; ^b 6.5 ^c	~90 ^e
1	6	15	175	~19	~0.025 mmol of Au NPs	nanoplatelets	wurtzite	~100 ^e
1	6	15	100	~19	~0.025 mmol of Au NPs	nanorods	19.0; ^a 4.8; ^b wurtzite	~45 ^e
1	6	15	100	~19	~5.5 mmol of HCl	nanorods	19.0; ^a 3.8; ^b 5.0; ^c wurtzite	~95 ^e

^a Rod length for nanorods. ^b Rod diameter for nanorods. ^c Aspect ratio for nanorods. ^d Edge length of cubes. ^e Here, yield refers to the fraction of the nanocrystals with the morphology listed in the column labeled as shape.

**Figure 1.** TEM image of CdS nanocrystals synthesized at 175 °C and a reaction time of ~3 h.

Results and Discussion

Effects of Temperature, Precursor Concentration, and Growth Time. The effects of precursor concentration, temperature, and growth time on the morphology of CdS NCs were considered first. Figure 1 shows a TEM image of CdS nanocrystals obtained after 3 h at 175 °C, using a 1:6 Cd/S molar ratio. The particles are ellipsoidal, with typical dimensions of about 12 nm. Further aging of the reaction system for an additional ~16 h produced polydisperse NCs of irregular shape, with typical dimensions ranging from 10 to 32 nm.

When the growth temperature was decreased from 175 to 100 °C, only rods, bipods, and tripods were produced, as shown in Figure 2. The fraction of the product consisting of CdS nanorods, bipods, tripods, and tetrapods was estimated to be 70, 19, 10, and 1%, respectively. This set of reaction conditions serves as the base case, from which a variety of modifications were made and to which the results were compared. The average length and diameter of the nanorods in Figure 2 were estimated to be 16.7 and 5.5 nm, respectively. The lattice fringes of the CdS nanorods are clearly shown in the inset, with fringe spacing of 3.3 Å. These

fringes, which correspond to (002) lattice planes for the wurtzite structure of CdS, are aligned perpendicular to the rod axis. Also, the HRTEM image of bipods indicates that the core has the cubic zinc blend structure with a tetrahedral geometry and lattice fringe spacing of 2.9 Å corresponding to the {200} planes.

At a growth temperature of 100 °C, increasing the precursor concentration resulted in the formation of tetrapods or particles with a “candy corn” morphology. As described previously, when 1 mmol of CdCl₂ and 6 mmol of sulfur were used in the reaction mixture (in 15 mL of oleylamine), the yield of tetrapods in the final product mixture was low. However, when the precursor concentration was increased by a factor of 2.5 and the total reaction volume was doubled (5 mmol of CdCl₂ and 30 mmol of sulfur in 30 mL of oleylamine), tetrapods dominated the nanocrystal product mixture, with up to ~65% of the product being nanotetrapods, as shown in Figure 3. The average length and diameter of the arms of these structures were estimated to be 21 and 6.3 nm, respectively.

When the precursor concentrations were changed to 10 mmol of CdCl₂ and 30 mmol of sulfur in 25 mL of oleylamine

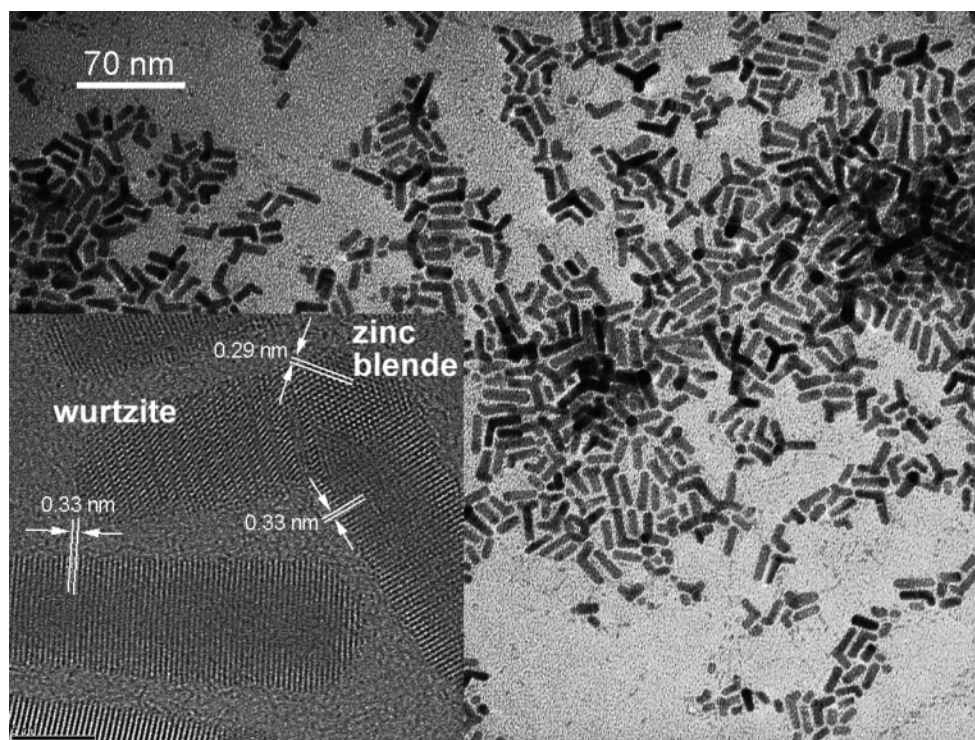


Figure 2. TEM and HRTEM (inset) images of CdS nanorods, bipods, and tripods synthesized at 100 °C and a reaction time of ~19 h. The scale bar in the inset is 5 nm. In the HRTEM, a tetrahedral zinc blend core with wurtzite arms growing from it is clearly visible.

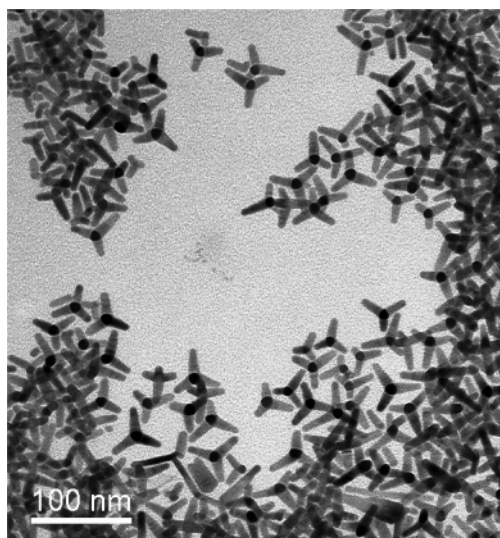


Figure 3. (a) TEM image of CdS tetrapods.

(decreasing the S/Cd ratio from 6:1 to 3:1), CdS nanocrystals with a “candy corn” morphology were produced, as shown in Figure 4. As shown there, CdS nanocrystals with the “candy corn” morphology made up about 80% of the nanocrystal product. These have an overall rod-like shape but with one end substantially larger in diameter than the other, perhaps reflecting an underlying tetrahedral structure. Bipods and tripods were also obtained but made up less than 10% of the nanocrystal population. The remainder of the particles consisted mainly of quasi-spherical and spherical NCs. The “candy corn”-shaped particles have an estimated average length of 24 nm.

Figure 5 shows the XRD patterns of the as-synthesized CdS nanocrystals produced at different temperatures and precursor concentrations. All of the diffraction peaks from the four samples can be readily indexed to wurtzite CdS. The relatively sharp {002} peak in patterns b–d, as compared to the corre-

sponding peak in pattern a, is consistent with the preferential [001] growth direction in the anisotropic CdS NCs. Examination of the powder XRD pattern of all four samples reveals the presence of the zinc blend crystal structure as well as the wurtzite crystal structure. This can be inferred from the intensity of the peaks corresponding to the {220} and {331} planes of the zinc blend structure, which also correspond to the {110} and {112} planes of the wurtzite structure, respectively. These are much more prominent than the wurtzite {103} peak that occurs between them. For pure bulk wurtzite CdS, the {103} peak intensity would be slightly greater than that of the neighboring {110} and {112} peaks, and a somewhat weaker {102} peak would appear at a 2θ value near 37°.

The results described previously illustrate the balance between kinetic and thermodynamic control that determines the final shape of CdS NCs.³² At relatively high temperature and low precursor concentrations, both surface diffusion and monomer desorption are favored. As a result, nuclei grow isotropically, leading to the formation of somewhat faceted quasi-spherical structures that minimize the surface energy for a given nanocrystal volume.³³ At longer reaction times and high temperatures, where monomer desorption is possible, the average nanocrystal size continues to increase via Ostwald ripening even after the limiting precursor has been depleted from solution. In contrast, at relatively low reaction temperature and higher precursor concentrations, the nanocrystal morphology is kinetically controlled. The nanocrystal grows preferentially in the kinetically most favorable direction, which is the one with the smallest activation barrier to the rate-limiting step(s) in the growth process. In the experiments described previously, at a higher growth temperature (~175 °C), the growth process appears to be under thermodynamic control. In this growth regime, isotropic growth is favorable, and therefore, quasi-spherical CdS NCs are obtained at an early stage of the reaction. High temperatures also lead to higher nucleation rates and therefore a larger number of nuclei since the activation energy for

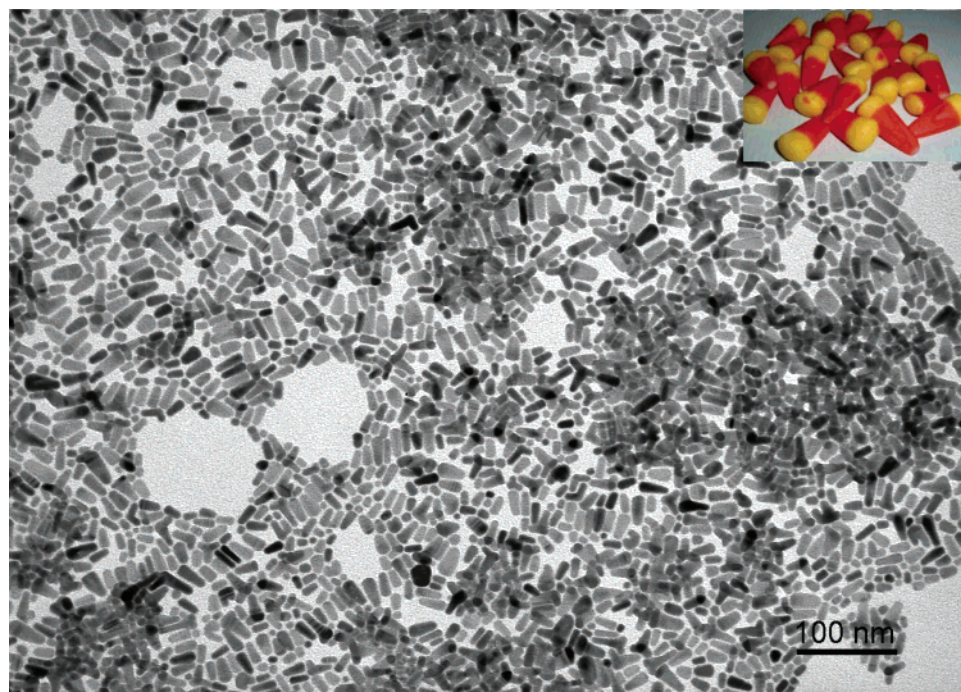


Figure 4. TEM image of CdS NCs with a “candy corn” morphology. The inset shows Brachs brand candy corn, for which this morphology is named.

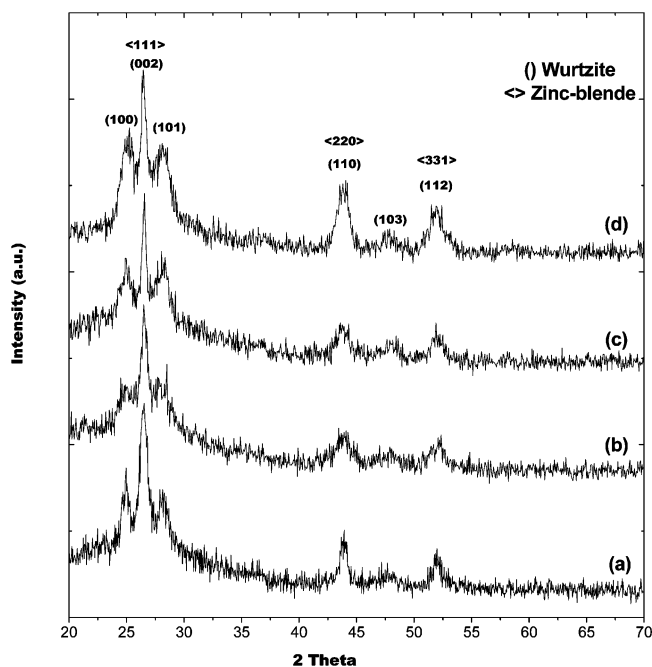


Figure 5. Powder X-ray diffraction of (a) quasi-spherical CdS NCs (as shown in Figure 1), (b) a mixture of CdS nanorods, bipods, and tripods (as shown in Figure 2), (c) CdS tetrapods (as shown in Figure 3), and (d) CdS nano-“candy corn” (as shown in Figure 4).

nucleation is generally higher than that for growth. These nuclei compete for the remaining precursor, resulting in fast depletion of it. Further aging of the system at high temperature promotes an Ostwald ripening process in which larger NCs grow at the cost of smaller ones, increasing both the average size and the polydispersity of the NCs.

Another important parameter that can control the shape of NCs is the crystallographic phase of the initial nuclei formed. For some NC systems, including CdS, the crystallographic phase of the nuclei depends on the temperature. CdS has two distinct crystalline phases: the cubic zinc blend phase that is stable

below 250 °C and the hexagonal wurtzite phase that is formed at high growth temperature (~300 °C).⁸ In this study, low temperatures were employed to produce non-spherical CdS NCs via kinetically controlled growth. At these relatively low temperatures, nucleation of tetrahedral NCs with the zinc blend structure, exposing four {111} faces, is more favorable than nucleation of NCs with the wurtzite structure. Subsequently, the epitaxial growth of the *c*-axis oriented wurtzite arms from four, three, two, or one of the equivalent {111} faces of the seed results in the formation of CdS tetrapods, tripods, bipods, or nanorods (or nano-“candy corn”), respectively. It appears that once the wurtzite arm nucleates on the zinc blend seed, its growth is relatively rapid. Thus, when a relatively low precursor concentration was used, the growth of CdS wurtzite arms did not occur on all the equivalent {111} faces of the zinc blend seeds, possibly due to the fast depletion of the limited precursor supply. In a perfectly stoichiometric tetrahedral nanocrystal terminated with {111} planes, different faces will have different surface terminations. For example, three Cd-terminated faces (with one dangling bond per Cd atom) and one S-terminated face (with three dangling bonds per S atom) is a possible configuration for a symmetric tetrahedron with the zinc blend structure and an equal number of Cd and S atoms. Thus, it is reasonable to expect that there may be different barriers to nucleation of the wurtzite phase on different faces of a tetrahedral zinc blend crystal. Once the formation of a wurtzite arm takes place on a {111} face of a zinc blend core, the growth rate on the (001) face of this wurtzite arm may be much faster than on the {111} surfaces of the zinc blend core. When a Cd/S ratio of 1:6 was used at the base case precursor concentrations, predominantly nanorods and bipods were produced, indicating that further growth of existing arms was substantially favored over nucleation of new arms. However, increasing the precursor concentrations by a factor of 2.5, while maintaining the 1:6 Cd/S molar ratio, produced predominantly tetrapods and tripods. The increased precursor concentration, corresponding to a higher precursor chemical potential (a larger chemical potential difference between precursor and nanocrystal), may have been

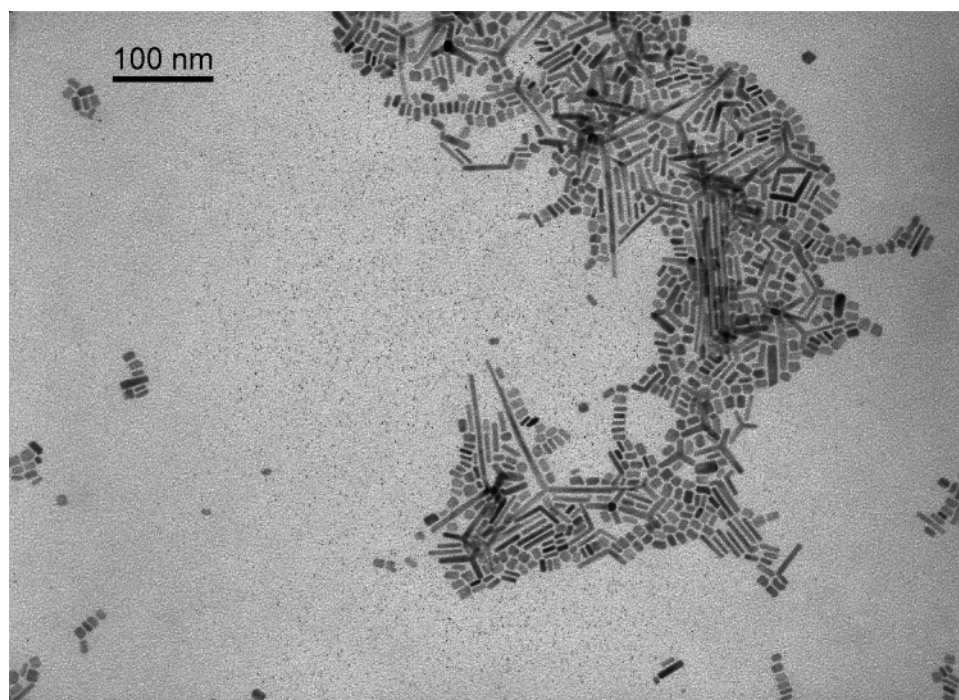


Figure 6. TEM image of CdS tetrapods with long wurtzite arms, accompanied by a larger number of nanorods and nanocubes.

sufficient to induce nucleation on faces where nucleation did not occur at the lower precursor concentration. An alternative explanation is that at higher concentrations, the ratio of precursors to zinc blend nuclei formed was higher, and therefore, more precursors were available to deposit on each nucleus. This explanation, however, would require that the concentration dependence of the number of nuclei formed be sublinear. This would be a very unusual result for homogeneous nucleation of a new phase but would be reasonable if the nucleation is somehow heterogeneously initiated.

A large excess of sulfur was used in all of the syntheses described previously. When a smaller amount of sulfur was used, the NC growth was more isotropic. In previous reports^{34,35} on the mechanism of CdSe quantum rod formation, the Cd/Se ratio was tuned to maintain a high Cd chemical potential. When the Cd precursor was used in excess, CdSe quantum rods were formed. In contrast, when the selenium precursor was used in excess, CdSe quantum dots were produced. Such results suggest that the less reactive species should be employed in excess to promote anisotropic growth of NCs. In the current studies, since the sulfur precursor complex is less reactive than the cadmium precursor complex, sulfur was added in excess.

Effects of Cosurfactants. In addition to the effects of temperature and precursor concentration on the morphologies of CdS NCs, the effect of the addition of tetradecylphosphonic acid (TDPA) as a cosurfactant was also investigated. Previous studies have reported that shape control of CdSe NCs can be achieved using phosphonic acids that strongly coordinate to Cd atoms and thereby slow the NC growth and result in preferential growth in the *c*-axis direction of the wurtzite crystal structure. Figure 6 shows the CdS NCs prepared in the presence of oleylamine and TDPA. The Cd/S molar ratio and TDPA concentration used for this synthesis were 1:3 and ~0.36 mmol (0.1 g), respectively. As shown in the TEM image, some CdS tripods with very long arms were produced, along with nanorods and nanocubes. The length of the wurtzite arms is estimated to be at least 100 nm. However, the yield of such long-armed tripods as compared to other shapes was relatively low (<10%). The CdS nanorods were predominant in the final product

(~70%). By varying the Cd/S molar ratio and the TDPA concentration, the system could be tuned to preferentially produce the CdS nanocubes. Figure 7 shows CdS nanocubes synthesized with a 1:6 Cd/S molar ratio and ~0.9 mmol (0.25 g) of TDPA. The yield of CdS nanocubes was estimated to be 85% of the total nanocrystal population. The cubes have an edge length of about 12 nm. The formation of long wurtzite arm tripods can be explained by presuming that TDPA increases the relative growth rate of the (001) face of hexagonal CdS that grows out of the (111) faces of the tetrahedral zinc blend core.^{36,37} The low yield of these long-armed tripods suggests that nucleation of wurtzite arms on the zinc blend cores occurs with low probability. Decreasing the cadmium precursor concentration while increasing the TDPA concentration may have promoted growth of the (111) faces of the zinc blend seeds rather than nucleation of wurtzite arms. That is, the probability of wurtzite arm nucleation is essentially reduced to zero. Rapid growth of a tetrahedral seed on its (111) faces, without growth on its (100) faces, will result in the (111) faces growing themselves out, producing a cubic overall shape. The powder XRD pattern from the nanocubes is shown in Figure 7b. It exhibits a relatively sharp peak corresponding to the zinc blend (111) planes and a large peak corresponding to the (220) planes. Peaks corresponding to the wurtzite (100), (101), and (103) planes are not present, or at least not visible above the noise level. This supports the conclusion that the nanocube samples are composed predominantly of the zinc blend phase.

In addition to the phosphonic acid, other cosurfactants including cetyltrimethylammonium bromide (CTAB) and trioctylphosphine oxide (TOPO) were also tested. Both of these surfactants have been widely used to synthesize metal and semiconductor NCs of controllable shape and size. For instance, water soluble non-spherical Au and CdS NCs were prepared in a CTAB micellar solution, where the CTAB micelle acts as a template for anisotropic growth of the NCs.^{21,38–40} On the other hand, non-spherical CdSe NCs have most often been fabricated by hot colloidal synthesis using trioctylphosphine (TOP) and/or trioctylphosphine oxide (TOPO) as the coordinating solvents as well as the directing agents.³⁷ When oleylamine

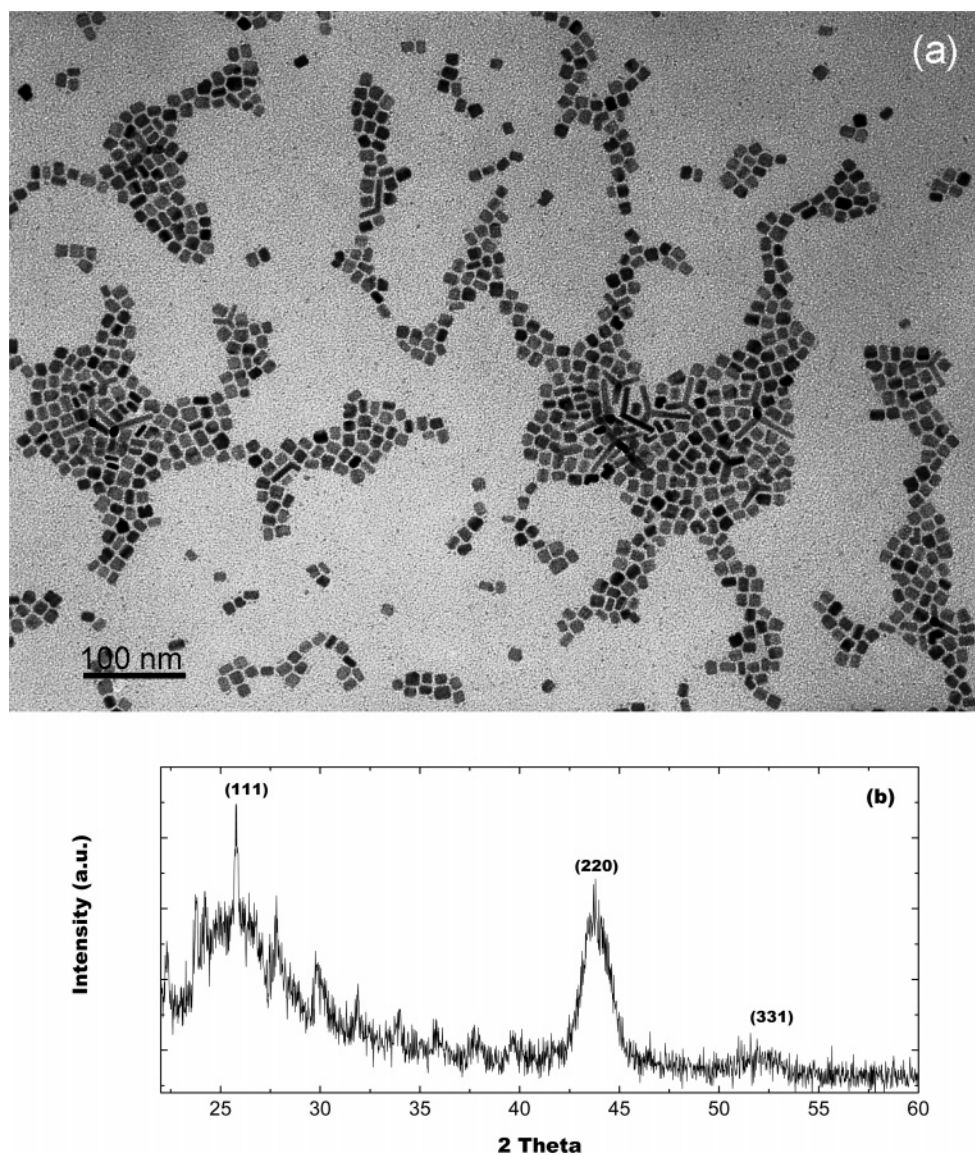


Figure 7. (a) TEM image of CdS nanocubes and (b) powder XRD from CdS nanocubes.

and CTAB were used as a binary surfactant mixture, CdS chain-like nanostructures were observed as shown in Figure 8. As seen in the HRTEM image, the CdS NCs are highly agglomerated and entangled, giving rise to the formation of chain-like structures. The lattice fringes are estimated to be 3.3 Å, which correspond to (200) lattice planes of the wurtzite structure. The different binding abilities of these two surfactants on different facets of CdS nanocrystals might have resulted in an oriented attachment-like mechanism⁴¹ that leads to fusion of the nanocrystals.

When a binary mixture of TOPO and oleylamine was used, predominantly, nanorods were observed, accompanied by some bipods and tripods (see Figure 9). The yields of nanorods, bipods, and tripods are estimated to be 90, 9, and 1%, respectively. The length and diameter of the nanorods are about 23.4 and 3.8 nm, giving an aspect ratio of ~ 6.2 . A drastic increase of the yield of nanorods was observed as compared to the base case using only oleylamine. This suggests that the presence of TOPO in oleylamine is promoting the growth of a single wurtzite arm from a zinc blend nucleus. TOPO molecules absorbed on the CdS nanocrystals may have greatly decreased the growth rate along the directions perpendicular to [002] growth direction of the CdS wurtzite arms. TOPO molecules may also bind more strongly than oleylamine on the {111}

surfaces of the zinc blend core, which inhibits the nucleation of the wurtzite phase on the remaining faces of the tetrahedral zinc blend crystal, favoring production of rods over bipods and tripods.

Effects of Au Nanoparticles. In previous work, we have synthesized PbSe⁴² and CdSe⁴³ quantum rods (QRs) and PbS nanowires⁴⁴ by using metal nanoparticles to seed the one-dimensional growth. For example, in the case of CdSe, we have found that multiple CdSe rods can nucleate and grow on a single gold nanoparticle seed. To investigate the effects of Au nanoparticle seeding on the CdS synthesis, ~ 4 nm gold nanoparticles containing ~ 0.025 mmol of gold atoms were added to a reaction mixture with a Cd/S ratio of 1:6 and aged at 175 °C for 19 h. Here, we refer to CdS nanocrystals seeded with Au nanoparticles as CdS(Au). Notably, when Au NPs were added, the product was composed of triangular, rectangular, pentagonal, and hexagonal CdS nanoplatelets that can form a two-dimensional nearly close-packed array as shown in Figure 10. In regions of this TEM image where a multilayer of NCs is present, many nanoplatelets are thin enough that the NCs in the underlying layer can be easily observed. Such faceted nanoplatelets of CdS were also produced by Cheng et al.,⁴⁵ under a different set of conditions. In the present case, the addition of gold NPs was required to promote the formation of nanoplate-

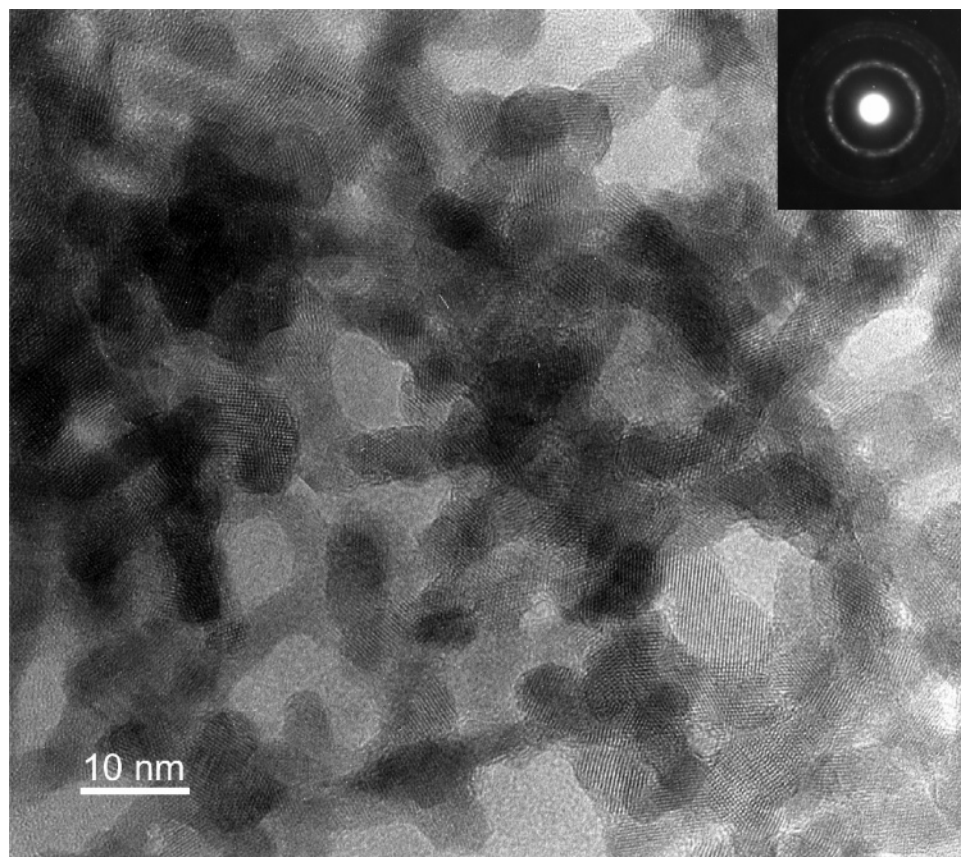


Figure 8. HRTEM image of CdS chain-like nanostructures.

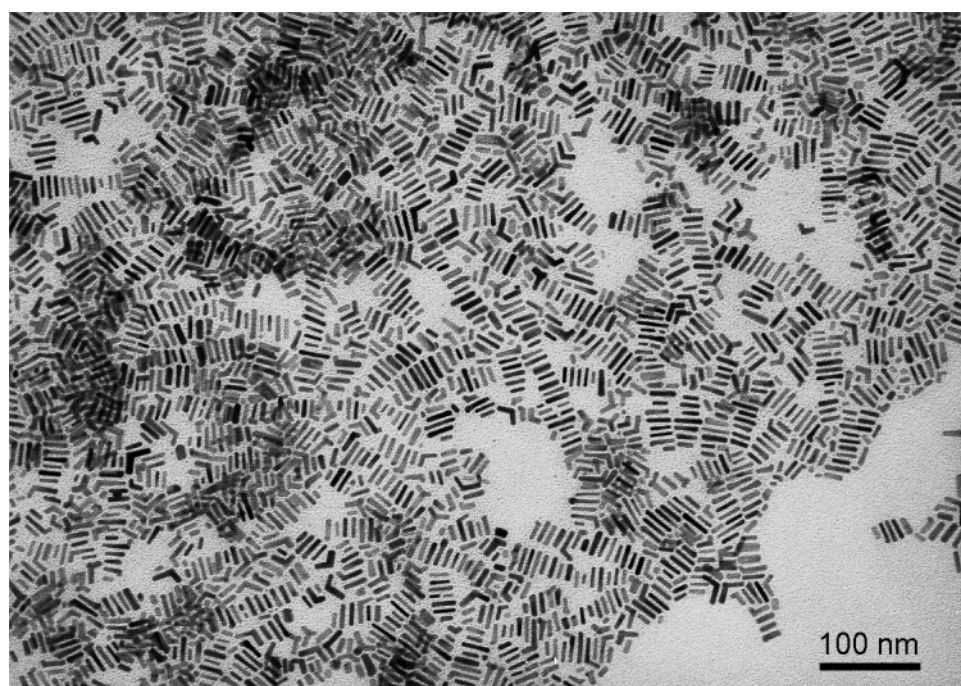


Figure 9. TEM image of CdS nanorods synthesized using a mixture of TOPO and oleylamine.

lets, and these formed at a relatively high concentration of sulfur precursor and long reaction time. This is in contrast to the synthesis method presented by Cheng et al.,⁴⁵ who reported that the faceted CdS nanocrystals were prepared at a much lower concentration of sulfur and in the absence of gold NPs. Direct comparisons between the two routes are difficult since they start from different sets of precursors, surfactants, and reaction conditions.

Decreasing the growth temperature from 175 to 100 °C using the same concentration of Au NPs and the same Cd/S molar ratio produced mainly nanorods, bipods, and quasi-spherical nanocrystals, as shown in Figure 11. The yields of CdS nanorods, bipods, and quasi-spherical NCs were estimated to be 45, 12, and 40%. Thus, a lower yield of nanorods was observed as compared to the base case (see Figure 3) where no Au NPs were added. The length and diameter of the nanorods

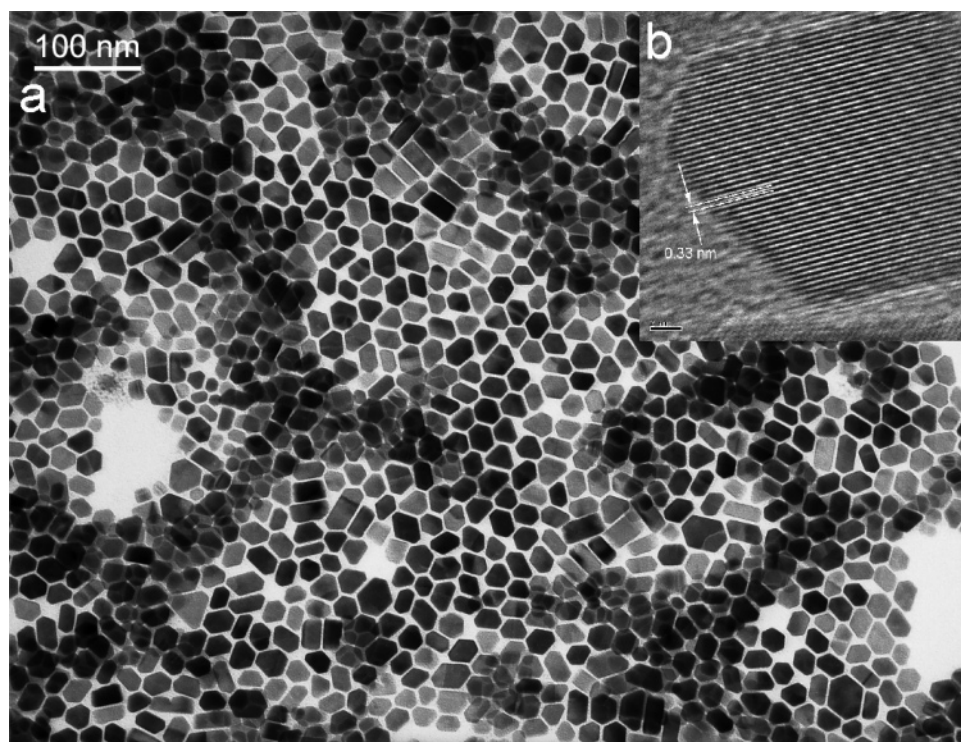


Figure 10. TEM image of CdS nanoplatelets.

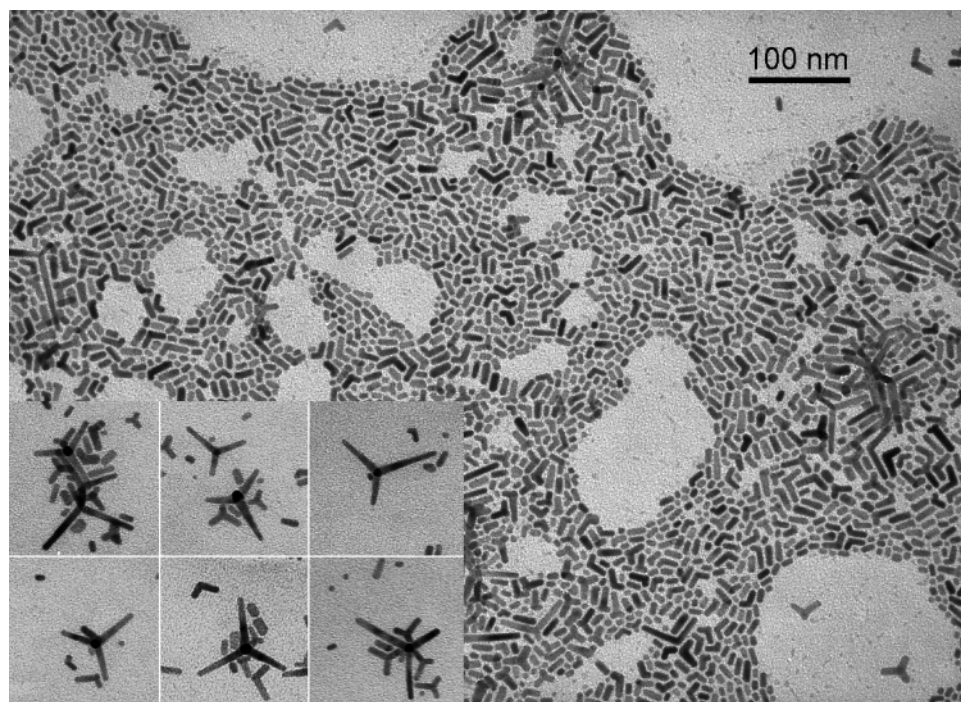


Figure 11. TEM image of CdS nanorods, bipods, and quasi-spherical dots.

are about 19 and 4.8 nm. The rest of the products mainly contain tripods and tetrapods. Even though the population of tetrapods produced in the presence of Au NPs was smaller than in their absence, it is still interesting to note that the CdS tetrapods synthesized in the presence of Au NPs have longer, higher aspect ratio arms than the CdS tetrapods produced without using Au NPs. As shown in the inset images of Figure 11, the average diameter and length of the arms from these tetrapods was estimated to be 5.6 and 38 nm, respectively, as compared to 6.3 and 21 nm when Au was not used (see Figure 3).

The XRD pattern from the CdS nanoplatelets is shown in Figure 12. All the peaks can be indexed to the wurtzite CdS

structure. The intensity of the (002) diffraction peak is much stronger than that of all other peaks, suggesting that the CdS nanoplatelets have a strong preferential orientation along the [001] direction. The HRTEM image of an individual CdS nanoplatelet shown in Figure 10b also demonstrates the crystallinity of these nanoplatelets. The lattice fringe spacing is 0.33 nm, corresponding to the (002) planes, confirming that the preferred growth direction is along the [001] direction. As discussed earlier, irregularly shaped polydispersed CdS NCs were obtained at 175 °C in the absence of Au NPs. The polydispersity of those NCs was attributed to an Ostwald ripening process. We might expect that, under these same

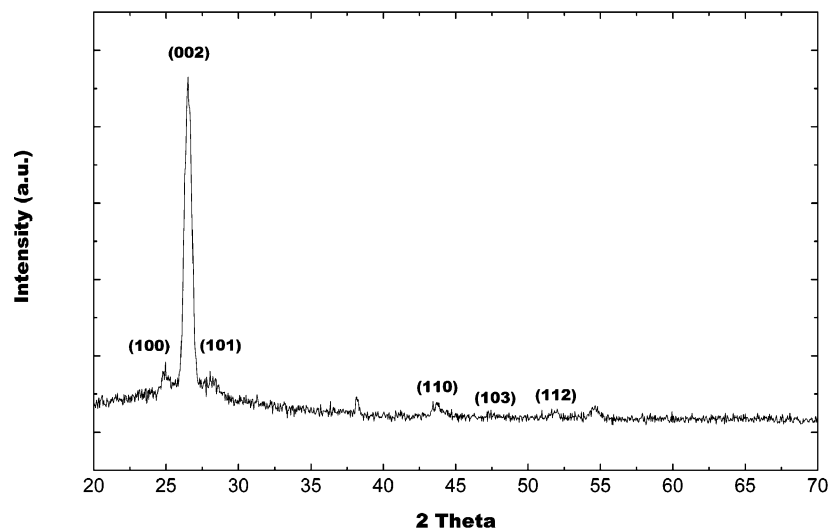


Figure 12. Powder X-ray diffraction pattern from CdS nanoplatelets.

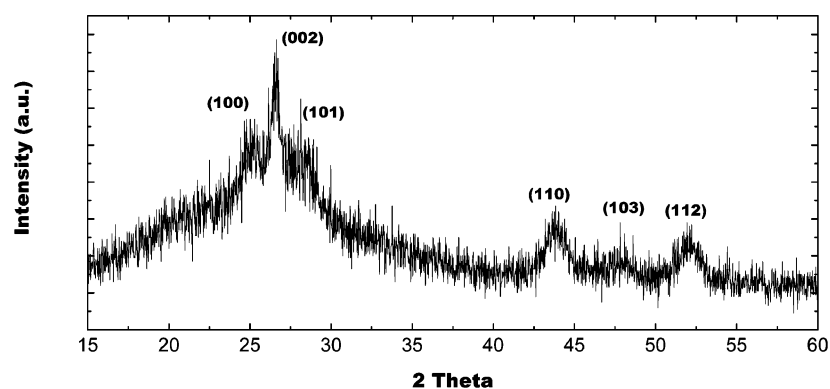


Figure 13. Powder X-ray diffraction pattern from CdS nanorods, bipods, and quasi-spherical dots produced in the presence of Au NPs.

conditions, a similar ripening process would convert the nanoplatelets into lower surface area, more nearly spherical structures. However, such ripening is not observed, suggesting that precursor desorption from these wurtzite nanoplatelets under these conditions is much slower than desorption from the irregular quasi-spherical NCs shown in Figure 1. Although the role of Au NPs in directing the growth of nanoplatelets is not fully understood, it appears that they induce nucleation of the wurtzite phase under conditions where the zinc blend phase would otherwise nucleate. Both XRD and HRTEM results confirm that the CdS nanoplatelets are predominantly wurtzite. Although wurtzite is the more stable bulk phase for CdS at all temperatures considered here, homogeneous nucleation of tetrahedral nuclei with the zinc blend crystal structure is favored by the facts that these tetrahedra expose only close-packed $\{111\}$ facets and that stoichiometric and complete tetrahedra can form for a large number of closely spaced cluster sizes (Cd_4S_4 , $\text{Cd}_{10}\text{S}_{10}$, $\text{Cd}_{20}\text{S}_{20}$, and $\text{Cd}_{35}\text{S}_{35}$, etc.). However, if the nanocrystals nucleate heterogeneously on a gold seed particle, then cleave from it, these factors will no longer be important, and the more stable wurtzite phase may form directly. At a lower reaction temperature of 100 °C and the same Au NP concentration, it appears that the nucleation of both wurtzite and zinc blend NCs is possible, which resulted in a combination of multipods and quasi-spherical NCs. The powder XRD pattern from this mixture of multipods and quasi-spherical NCs is shown in Figure 13. This pattern is similar to those shown in Figure 4 and suggests that both zinc blend and wurtzite phases are present.

Effects of Acid. Recently, it was reported that mainly CdSe tetrapods were formed in a hot colloidal reaction in the presence

of acids such as HCl and H_2SO_4 .⁴⁶ In that study, the role of acid was demonstrated by the fact that only dot-shaped CdSe NCs formed in the absence of acid. It was suggested that the effect of the acidic environment in the reaction system was to promote the growth of the zinc blend seeds and subsequently influence the growth rates of different crystal facets and thereby promote anisotropic growth of CdSe nanocrystals. To investigate the effects of an acidic environment on the formation of CdS NCs, we have added HCl (~ 5.5 mmol) into the base case reaction system. This resulted in a high yield of uniform CdS nanorods as illustrated in Figure 14. The yield of nanorods is estimated to be $\sim 95\%$ of the total NC population. The length and diameter of the nanorods are about 19 and 3.8 nm, corresponding to an aspect ratio of ~ 5 . Compared to the synthesis of nanorods by an identical procedure without the use of acid, a 25% increase in the yield of nanorods was observed. The length distribution of the nanorods produced in the presence of HCl is much narrower than that of nanorods synthesized in the absence of HCl as well as the ones prepared using a binary surfactant mixture of TOPO and oleylamine.

In the case of formation of CdSe tetrapods,⁴⁶ it was suggested that the proton (H^+) increases the yield of zinc blend nuclei and then may be adsorbed on facets other than the four $\{111\}$ facets. As a result, the growth can only continue on the four equivalent $\{111\}$ facets. As discussed previously, for the CdS synthesis described here, nucleation of the zinc blend phase is already favorable at low temperatures in the absence of acid. In this system, the greatest effect of acid addition seems to be to suppress the formation of bipods and tripods. Careful analysis of the TEM images shows that the yield of bipods and tripods

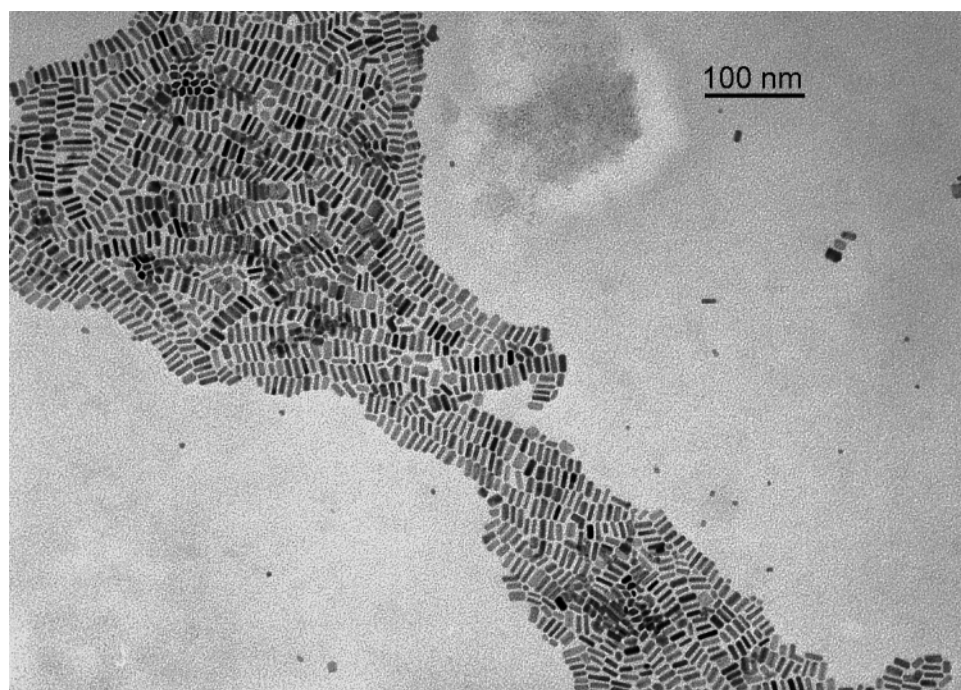


Figure 14. TEM image of uniform CdS nanorods produced in the presence of HCl.

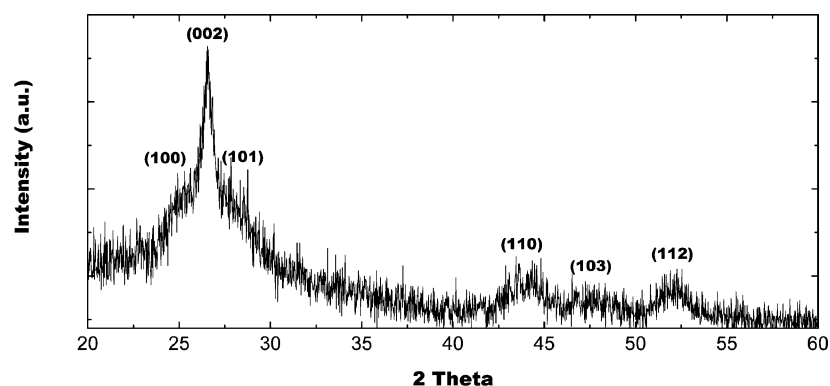


Figure 15. Powder X-ray diffraction pattern of CdS nanorods produced with addition of HCl.

is less than 0.5%, suggesting that formation of multipods based on zinc blend seeds is unfavorable in the presence of HCl. The suppression of multipod formation may be due to direct nucleation of the wurtzite phase in the presence of acid. Figure 15 shows the powder XRD pattern from CdS nanorods like those shown in Figure 14. Comparing this diffraction pattern to those in Figure 4, we see a higher ratio of the (103) peak to the (110) and (112) peaks, suggesting a higher wurtzite phase fraction. The (002) wurtzite peak is substantially narrow than all other peaks, consistent with growth along the *c*-axis of the wurtzite structure. In this system, H⁺ may passivate faces other than the growing {001} faces, which are structurally similar to the zinc blend {111} facets of the same polarity, leading to growth along the [001] direction. However, since anisotropic growth occurs in this system even without acid addition, the effect is less clear than for the CdSe system.

Figure 16 shows the UV absorption and PL spectra, in hexane, of the largely monodispersed CdS nanorods produced in the presence of HCl. The absorption spectrum shows an excitonic peak around 470 nm, which is blue-shifted from the bulk band gap value (CdS, 517 nm) due to quantum confinement in the transverse direction. The PL spectrum of the monodispersed CdS nanorods shows a band edge emission at 482 nm. The photoluminescence (PL) quantum yield (QY) of the CdS nanorods is estimated to be ~0.05%. The low QY is not

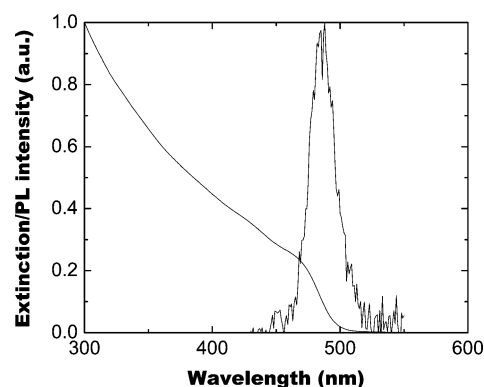


Figure 16. UV-vis absorption and PL spectra of monodispersed CdS nanorods like those shown in Figure 14.

surprising because of the expected reduced quantum confinement in the rod-shaped nanocrystals accompanied by little band edge and mostly trap state emissions.

Conclusion

In summary, we have presented a comprehensive study of a simple but versatile solution-phase method for synthesizing different shapes of high-quality CdS NCs at low temperature

(<175 °C and in most cases 100 °C). The shapes of CdS NCs have been systematically modulated by tuning the reaction parameters (e.g., temperature and precursor concentrations) or introducing suitable additives (e.g., cosurfactants, metal nanoparticles, or acid) into the reaction mixture, while keeping the principal reagents and reaction conditions otherwise fixed. This study underscores the sensitive dependence of nanocrystal shapes and sizes on the reaction parameters. It demonstrates the possibilities for manipulating nanocrystal synthetic parameters to produce custom tailored shapes for prospective nanostructured devices. In particular, it was shown that acidification of the reaction medium or addition of gold nanoparticles can lead to the nucleation of the wurtzite polymorph under conditions where nucleation of the zinc blend phase would otherwise be favored. Under most conditions where the zinc blend phase nucleates first, there is a subsequent transition to growth of the wurtzite polymorph, leading to growth of rods or multipods (bipods, tripods, and tetrapods) with a tetrahedral zinc blend core and wurtzite arms. In the presence of tetradecylphosphonic acid, at some conditions, it was possible to avoid this transition to wurtzite growth and achieve nearly pure zinc blend nanocrystals that assumed a cubic morphology.

Acknowledgment. This work was supported in part by the Chemistry and Life Sciences Directorate of the Air Force Office of Scientific Research (Grant FA95550-06-1-0398). We also thank the National Center for Electron Microscopy at Lawrence Berkeley National Laboratory for providing access to the HRTEM facility.

References and Notes

- (1) Murray, C. B.; Kagan, C. R.; Bawendi, M. G. *Ann. Rev. Mater. Sci.* **2000**, *30*, 545–610.
- (2) Zhang, J. Z. *J. Phys. Chem. B* **2000**, *104*, 7239–7253.
- (3) Shen, G.; Cho, J. H.; Yoo, J. K.; Yi, G.-C.; Lee, C. J. *J. Phys. Chem. B* **2005**, *109*, 9294–9298.
- (4) Mandal, S.; Rautaray, D.; Sanyal, A.; Sastry, M. *J. Phys. Chem. B* **2004**, *108*, 7126–7131.
- (5) Weinhardt, L.; Gleim, T.; Fuchs, O.; Heske, C.; Umbach, E.; Bar, M.; Muffler, H.-J.; Fischer, C.-H.; Lux-Steiner, M. C.; Zubavichus, Y.; Niesen, T. P.; Karg, F. *Appl. Phys. Lett.* **2003**, *82*, 571–573.
- (6) Yang, J.; Zeng, J.-H.; Yu, S.-H.; Yang, L.; Zhou, G.-E.; Qian, Y.-T. *Chem. Mater.* **2000**, *12*, 3259–3263.
- (7) Yang, C.-S.; Awschalom, D. D.; Stucky, G. D. *Chem. Mater.* **2002**, *14*, 1277–1284.
- (8) Jun, Y.-w.; Lee, S.-M.; Kang, N.-J.; Cheon, J. *J. Am. Chem. Soc.* **2001**, *123*, 5150–5151.
- (9) Li, Y.-D.; Liao, H.-W.; Ding, Y.; Qian, Y.-T.; Yang, L.; Zhou, G.-E. *Chem. Mater.* **1998**, *10*, 2301–2303.
- (10) Cao, Y. C.; Wang, J. *J. Am. Chem. Soc.* **2004**, *126*, 14336–14337.
- (11) Zhang, Z. H.; Chin, W. S.; Vittal, J. J. *J. Phys. Chem. B* **2004**, *108*, 18569–18574.
- (12) Xue, P.; Lu, R.; Huang, Y.; Jin, M.; Tan, C.; Bao, C.; Wang, Z.; Zhao, Y. *Langmuir* **2004**, *20*, 6470–6475.
- (13) Barrelet, C. J.; Wu, Y.; Bell, D. C.; Lieber, C. M. *J. Am. Chem. Soc.* **2003**, *125*, 11498–11499.
- (14) Xu, D.; Liu, Z.; Liang, J.; Qian, Y. *J. Phys. Chem. B* **2005**, *109*, 14344–14349.
- (15) Ye, C.; Meng, G.; Wang, Y.; Jiang, Z.; Zhang, L. *J. Phys. Chem. B* **2002**, *106*, 10338–10341.
- (16) Pan, A.; Liu, R.; Yang, Q.; Zhu, Y.; Yang, G.; Zou, B.; Chen, K. *J. Phys. Chem. B* **2005**, *109*, 24268–24272.
- (17) Kar, S.; Chaudhuri, S. *J. Phys. Chem. B* **2006**, *110*, 4542–4547.
- (18) Wang, Y.; Meng, G.; Zhang, L.; Liang, C.; Zhang, J. *Chem. Mater.* **2002**, *14*, 1773–1777.
- (19) Thiruvengadathan, R.; Regev, O. *Chem. Mater.* **2005**, *17*, 3281–3287.
- (20) Zhang, M.; Drechsler, M.; Muller, A. H. E. *Chem. Mater.* **2004**, *16*, 537–543.
- (21) Chen, C.-C.; Chao, C.-Y.; Lang, Z.-H. *Chem. Mater.* **2000**, *12*, 1516–1518.
- (22) Zhang, P.; Gao, L. *Langmuir* **2003**, *19*, 208–210.
- (23) Simmons, B. A.; Li, S.; John, V. T.; McPherson, G. L.; Bose, A.; Zhou, W.; He, J. *Nano Lett.* **2002**, *2*, 263–268.
- (24) Panda, A. B.; Glaspell, G.; El-Shall, M. S. *J. Am. Chem. Soc.* **2006**, *128*, 2790–2791.
- (25) Shieh, F.; Saunders, A. E.; Korgel, B. A. *J. Phys. Chem. B* **2005**, *109*, 8538–8542.
- (26) Chae, W.-S.; Shin, H.-W.; Lee, E.-S.; Shin, E.-J.; Jung, J.-S.; Kim, Y.-R. *J. Phys. Chem. B* **2005**, *109*, 6204–6209.
- (27) Chu, H.; Li, X.; Chen, G.; Zhou, W.; Zhang, Y.; Jin, Z.; Xu, J.; Li, Y. *Cryst. Growth Des.* **2005**, *5*, 1801–1806.
- (28) Zhang, J.; Jiang, F.; Zhang, L. *J. Phys. Chem. B* **2004**, *108*, 7002–7005.
- (29) Brust, M.; Walker, M.; Bethell, D.; Schiffrin, D. J.; Whyman, R. *J. Chem. Soc., Chem. Commun.* **1994**, 802–803.
- (30) Daniel, M.-C.; Astruc, D. *Chem. Rev.* **2004**, *104*, 293–346.
- (31) Joo, J.; Na, H. B.; Yu, T.; Yu, J. H.; Kim, Y. W.; Wu, F.; Zhang, J. Z.; Hyeon, T. *J. Am. Chem. Soc.* **2003**, *125*, 11100–11105.
- (32) Jun, Y.-W.; Lee, J.-H.; Choi, J.-S.; Cheon, J. *J. Phys. Chem. B* **2005**, *109*, 14795–14806.
- (33) Lee, S.-M.; Cho, S.-N.; Cheon, J. *Adv. Mater.* **2003**, *15*, 441–444.
- (34) Peng, Z. A.; Peng, X. *J. Am. Chem. Soc.* **2001**, *123*, 1389–1395.
- (35) Peng, Z. A.; Peng, X. *J. Am. Chem. Soc.* **2002**, *124*, 3343–3353.
- (36) Manna, L.; Milliron, D.; Meisel, A.; Scher, E.; Alivisatos, A. P. *Nat. Mater.* **2003**, *2*, 382–385.
- (37) Manna, L.; Scher, E. C.; Alivisatos, A. P. *J. Am. Chem. Soc.* **2000**, *122*, 12700–12706.
- (38) Curri, M. L.; Agostiano, A.; Manna, L.; Monica, M. D.; Catalano, M.; Chiavarone, L.; Spagnolo, V.; Lugara, M. *J. Phys. Chem. B* **2000**, *104*, 8391–8397.
- (39) Tao, C.; Zheng, S.; Mohwald, H.; Li, J. *Langmuir* **2003**, *19*, 9039–9042.
- (40) Chen, H. M.; Peng, H. C.; Liu, R. S.; Asakura, K.; Lee, C. L.; Lee, J. F.; Hu, S. F. *J. Phys. Chem. B* **2005**, *109*, 19553–19555.
- (41) Yu, J. H.; Joo, J.; Park, H. M.; Baik, S.-I.; Kim, Y. W.; Kim, S. C.; Hyeon, T. *J. Am. Chem. Soc.* **2005**, *127*, 5662–5670.
- (42) Yong, K.-T.; Sahoo, Y.; Choudhury, K. R.; Swihart, M. T.; Minter, J. R.; Prasad, P. N. *Nano Lett.* **2006**, *6*, 709–714.
- (43) Yong, K.-T.; Sahoo, Y.; Swihart, M. T.; Prasad, P. N. *Adv. Mater.* **2006**, *18*, 1978–1982.
- (44) Yong, K.-T.; Sahoo, Y.; Choudhury, K. R.; Swihart, M. T.; Minter, J. R.; Prasad, P. N. *Chem. Mater.* **2006**, *18*, 5965–5972.
- (45) Cheng, Y.; Wang, Y.; Bao, F.; Chen, D. *J. Phys. Chem. B* **2006**, *110*, 9448–9451.
- (46) Pang, Q.; Zhao, L. J.; Cai, Y.; Nguyen, D. P.; Regnault, N.; Wang, N.; Yang, S. H.; Ge, W. K.; Ferreira, R.; Bastard, G.; Wang, J. N. *Chem. Mater.* **2005**, *17*, 5263–5267.